Acta Biomaterialia 126 (2021) 394–407

Contents lists available at ScienceDirect

Acta Biomaterialia

journal homepage: www.elsevier.com/locate/actbio

Full length article

Delivery of cardiovascular progenitors with biomimetic microcarriers reduces adverse ventricular remodeling in a rat model of chronic myocardial infarction

E. Garbayo[a,b], A. Ruiz-Villalba[b,c,d,e,1], S.C. Hernandez[b,c,1], L. Saludas[a], G. Abizanda[b,c], B. Pelacho[b,c], C. Roncal[b,f,g], B. Sanchez[h], I. Palacios[h], F. Prósper[b,c,i,*], M.J. Blanco-Prieto[a,b,*]

[a] Department of Pharmaceutical Technology and Chemistry, School of Pharmacy and Nutrition, University of Navarra, Pamplona, Spain
[b] Instituto de Investigación Sanitaria de Navarra (IdiSNA), Pamplona, Spain
[c] Program of Regenerative Medicine, CIMA, University of Navarra, Pamplona, Spain
[d] Department of Animal Biology, Institute of Biomedicine of Málaga (IBIMA) Faculty of Science, University of Málaga, Málaga, Spain
[e] Andalusian Centre for Nanomedicine and Biotechnology (BIONAND), Málaga, Spain
[f] Laboratory of Atherothrombosis, Program of Cardiovascular Diseases, Cima Universidad de Navarra, Pamplona, Spain
[g] CIBERCV, Carlos III Institute of Health, Madrid, Spain
[h] Tigenix-Takeda, Madrid, Spain
[i] Centro de Investigación Biomédica en Red (CIBERONC), Madrid, Spain

ARTICLE INFO

Article history:
Received 9 November 2020
Revised 5 February 2021
Accepted 5 March 2021
Available online 11 March 2021

Keywords:
Cardiac repair
Chronic myocardial infarction
Cardiovascular progenitors
Biomimetic microparticles
Extracellular vesicles
Ventricular remodeling

ABSTRACT

Despite tremendous progress in cell-based therapies for heart repair, many challenges still exist. To enhance the therapeutic potential of cell therapy one approach is the combination of cells with biomaterial delivery vehicles. Here, we developed a biomimetic and biodegradable micro-platform based on polymeric microparticles (MPs) capable of maximizing the therapeutic potential of cardiac progenitor cells (CPCs) and explored its efficacy in a rat model of chronic myocardial infarction. The transplantation of CPCs adhered to MPs within the infarcted myocardial microenvironment improved the long-term engraftment of transplanted cells for up to one month. Furthermore, the enhancement of cardiac cellular retention correlated with an increase in functional recovery. In consonance, better tissue remodeling and vasculogenesis were observed in the animals treated with cells attached to MPs, which presented smaller infarct size, thicker right ventricular free wall, fewer deposition of periostin and greater density of vessels than animals treated with CPCs alone. Finally, we were able to show that part of this beneficial effect was mediated by CPC-derived extracellular vesicles (EVs). Taken together, these findings indicate that the biomimetic microcarriers support stem cell survival and increase cardiac function in chronic myocardial infarction through modulation of cardiac remodeling, vasculogenesis and CPCs-EVs mediated therapeutic effects. The biomimetic microcarriers provide a solution for biomaterial-assisted CPC delivery to the heart.

Statement of significance

In this study, we evaluate the possibility of using a biomimetic and biodegradable micro-platform to improve cardiovascular progenitor therapy. The strategy reported herein serves as an injectable scaffold for adherent cells due to their excellent injectability through cardiac catheters, capacity for biomimetic three-dimensional stem cell support and controllable biodegradability. In a rat model of chronic myocardial infarction, the biomimetic microcarriers improved cardiac function, reduced chronic cardiac remodeling and increased vasculogenesis through the paracrine signaling of CPCs. We have also shown that extracellular vesicles derived from CPCs cultured on biomimetic substrates display antifibrotic effects, playing an important role in the therapeutic effects of our tissue-engineered approach. Therefore, biomimetic microcarriers represent a promising and effective strategy for biomaterial-assisted CPC delivery to the heart.

* Corresponding authors.
E-mail addresses: fprosper@unav.es (F. Prósper), mjblanco@unav.es (M.J. Blanco-Prieto).

[1] A. Ruiz-Villalba and S.C. Hernandez contribute equally to this manuscript.

https://doi.org/10.1016/j.actbio.2021.03.017

1. Introduction

Myocardial infarction (MI) is the leading cause of morbidity and mortality worldwide [1]. Although pharmacological and interventional strategies have been developed, they fail to restore the lost cardiac tissue and are only useful to alleviate some of the symptoms of heart failure. As an alternative, cardiac cell therapy aims to counteract the loss of cardiomyocytes by repopulating the ischemic myocardium with cells with a regenerative capacity [2,3]. Different stem/progenitor cells have been transplanted into the infarcted heart with the hope that these cells would engraft, differentiate and proliferate to form new functional myocardium [4]. Among them, cardiac progenitor cells (CPCs) are particularly promising, since they have proved therapeutic efficacy in animal models and clinical trials [5–7]. Their properties indicate that CPCs could be an ideal cell source for cardiac tissue engineering. Although the exact mechanism by which CPCs promotes a beneficial effect is not fully understood, there is a general agreement that it involves paracrine secretions rather than engraftment and differentiation [4,8]. Among these approaches, extracellular vesicles (EVs) have recently been at the center of attention due to their capacity to recapitulate the benefits of the injected progenitor cells, including cardiac function improvement, cardiomyocyte survival and proliferation and antifibrotic effects [9–13].

Despite the potential of stem cell therapy, it is necessary to optimize cell engraftment, survival and functionality post-transplantation to achieve better outcomes. Several studies have found that the combination of cells with biomaterials enhances the benefits of cardiac cell therapy [14]. Moreover, it is also critical to develop better scaffolds that improve not only cell delivery, but also cellular behavior, function and survival. In particular, hydrogels and cardiac patches have been explored in preclinical studies to deliver and retain cells in the infarcted myocardium, bringing significant advances in cardiac function [15–17]. However, their clinical translation has been limited due to difficulties injecting them through cardiac catheters. In this context, the use of biodegradable and biocompatible microcarriers based on polymeric microparticles (MPs) could improve cell-delivery challenges. Over the past decades, MPs have been mostly investigated as reservoirs for protein and drug delivery [18,19]. Additionally, this system can also be used as an injectable particulate scaffold for adherent cells due to their excellent injectability through minimally invasive catheter technology, capacity for tridimensional stem cell support and controllable biodegradability [14,20,21]. Moreover, MP surface can be functionalized with extracellular matrix molecules (ECM) such as collagen, fibronectin and laminin to create biomimetic microcarriers that favor the proliferation, differentiation and function of the transplanted cells. Remarkably, MPs are particularly relevant in the preparation of both bottom-up and top-down tissue engineering strategies or as reinforcement units in bioinks for 3D bioprinting, being a very versatile platform for a variety of biomanufacturing applications [22].

This study was designed to determine whether biomimetic microcarriers might improve CPC therapy in a rat model of chronic MI leading to enhanced cell engraftment, cardiac function and remodeling. The cellular and molecular mechanisms by which this strategy may promote tissue repair were also evaluated. Altogether, our novel findings demonstrate that biomimetic microcarriers support cell survival and increase cardiac function in chronic MI through modulation of cardiac remodeling, vasculogenesis and CPCs-EVs mediated therapeutic effects. Therefore, biomimetic microcarriers can improve current cell therapy strategies with CPCs and they represent a potential approach for biomaterial-assisted CPCs delivery to the heart.

2. Materials and methods

2.1. Isolation, culture and characterization of CPCs

CPC isolation from adult male Wistar rat hearts, their characterization and green fluorescent protein (GFP) lentiviral transduction were performed by Coretherapix SLU as previously reported [23,24]. Briefly, hearts of male Wistar rats were digested by enzymatic digestion (Collagenase Type 2, Worthington) and mechanical dissociation to obtain a single cell suspension. This suspension was immunoselected for c-kit$^+$/CD45$^-$ cells using magnetic microbeads coupled with antibodies (Miltenyi). Then, cells were cultured in a 0.1% (w/v) gelatin-coated (Sigma-Aldrich) flask in low O_2 conditions (3%) at a density of 3000–5000 cells/cm^2 using DMEM/F12 (Life Technology) and neurobasal medium (Life Technology) (1:1) supplemented with 10% FBS (Biochrom), 1% P/S (Life Technology), 1% L-Glu (Life Technology), 0.5% insulin-transferrin-selenium (ITS) (Life Technology), growth factors (basic Fibroblasts Growth Factor (bFGF) (10 ng/mL) (Peprotech), IGF-II (30 ng/mL) (Peprotech), EGF (20 ng/mL) (Peprotech), LIF (10 ng/mL) (Millipore)) together with 1% B-27 (Life Technology), 0.5% N-2 (Life Technology) and β-mercaptoethanol (50 µM) (Sigma-Aldrich) (CSCs medium). Concerning the markers expressed by these cells, a flow cytometry study was performed after four passages in culture, and rat CPCs were positive for CD44, CD166, CD90 and Sca-1 and negative for CD45, CD34 and CD117 (c-kit).

2.2. Preparation and characterization of MPs

Poly(lactic-co-glycolic acid) (PLGA) MPs were prepared by the multiple emulsion solvent evaporation method using the Total Recirculation One Machine System (TROMS). Briefly, the organic phase (o) consisting of 50 mg PLGA Resomer® RG 503H (Mw: 34 kDa) (Boehringer-Ingelheim) dissolved in a mixture of 4 mL acetone/dichloromethane (1:3) (Panreac Quimica S.A.) was injected into the inner aqueous phase (w_1) formed by 5 mg human serum albumin (Sigma-Aldrich), 5 μL PEG 400 (Sigma-Aldrich), and 200 μL phosphate-buffered saline (PBS) pH 7.4. The w_1/o emulsion was allowed to recirculate through the system for 1 min and 30 s. Then this emulsion was added to the outer aqueous phase (w_2) consisting of 20 mL 0.5% poly (vinyl alcohol) 88% hydrolyzed (MW 125 kDa) (Polysciences) and allowed to recirculate for 2 min and 30 s. Finally, the w_1/o/w_2 emulsion was stirred at room temperature for 3 h to allow total solvent evaporation. For fluorescence-labeled microparticles, rhodamin B isothiocyanate (0.5 mg/mL) (Sigma-Aldrich) was added to the inner aqueous phase and microspheres were prepared as described above. MPs were washed three times with ultrapure water by consecutive centrifugation at 20,000 g at 4 °C for 5 min and lyophilized without cryoprotective agents for 48 h (Genesis Freeze Dryer 12EL; VirTis, Gardiner, NY). Lyophilized MPs were stored at 4 °C.

Particle size and size distribution were measured by laser diffractometry using a Mastersizer (Malvern Instruments, Malvern, UK). MPs were dispersed in ultrapure water and analyzed under continuous stirring. The average particle size was expressed as the volume mean diameter. Particle surface charge was determined by Z potential measurement using a Zetasizer Nano ZS (Malvern Instruments), based on the analysis of complete electrophoretic mobility distributions.

2.3. MP surface coating

To facilitate the adhesion of CPCs to MPs, the particle surface was functionalized by coating with biomimetic molecules. Colla-

gen type 1 of rat tail 3 mg/mL (Gibco-Invitrogen), the major protein component of the cardiac extracellular matrix, and poly-D-lysine (PDL) (Sigma-Aldrich), a synthetic amino acid chain, were physically adsorbed onto the surface of PLGA MPs. Particle coating was performed in Sigmacote-coated tubes (Sigma-Aldrich). Briefly, 5 mg MPs were first dispersed in acidic PBS (pH 5.7). Then, biomimetic molecules (0.2 μg/cm^2 collagen and 0.3 μg/cm^2 PDL) were added to the particle solution and mixed with the particles under rotation at room temperature for 60 min. Coated MPs were subsequently rinsed with distilled sterile water by consecutive centrifugations (25,000 g, 4 °C, 10 min) and lyophilized for 48 h before use. Z potential of biomimetic MPs was measured to confirm that the particles had been successfully coated.

2.4. CPC attachment to MPs

The culture of CPCs with biomimetic microcarriers was performed in Costar® Ultra-Low cluster flat-bottom sterile polystyrene plates (Merck), designed to avoid attachment of cells to the plate. For the adhesion of cells, 0.75 mg coated MPs were dispersed in cell culture medium before the addition of 1×10^6 CPCs (seeding density of 2000 cells/cm^2). The mixture was flushed, plated in the Costar® Ultra-Low attachment plates and incubated at 37 °C. No agitation was used to allow CPCs to settle and attach to the microcarriers. The evolution of cell adhesion to MPs was assessed by bright-field microscopy (Nikon TMS, Amsterdam, The Netherlands) at different time points (0, 10, 30, 60 and 90 min).

2.5. In vivo *studies using a rat MI model*

All animal procedures were approved by the Institutional Animal Care and Use Committee of the University of Navarra and were performed according to the requirements of EU legislation.

MI was performed as previously described by our group [25,26]. A total of 40 Sprague-Dawley rats (Harlan-IBERICA, Spain) underwent permanent occlusion of the left anterior descending coronary artery. CPCs (1×10^6 cells/80 μL injection medium, n = 16) or CPCs-MPs (1×10^6 cells adhered to 0.75 mg biomimetic MPs/80 μL injection medium, n = 17) were injected in a blinded manner four weeks post-MI among the surviving animals (n = 33). Cell injections were delivered intramyocardially in 2 different areas of the infarct zone using a 27G syringe.

2.6. Assessment of CPC survival, engraftment and proliferation

The survival and engraftment of injected cells were analyzed and quantified at 24 h, 7, 14 and 30 days after treatment by immunofluorescence against GFP (Abcam ab290, 1:500) following conventional procedures. The number of engrafted cells was calculated by quantifying images from 5 to 6 serial heart sections 50 μm apart and extrapolating this number to the whole length of the graft area. Data were expressed as the percentage of the number of engrafted *versus* injected cells. Images were acquired using a camera attached to a Zeiss Axio Imager M1 fluorescence microscope. The proliferation of transplanted cells at 7 days after treatment was investigated by double staining for GFP (Abcam ab290, 1:500) and proliferative marker Ki67 (BD Pharmingen™ 558615, 1:10). The number of proliferative GFP$^+$ cells was quantified in 100 cells per section, in 4 sections per animal. Data were expressed as the percentage of proliferative cells from total cells. All images were acquired using a camera attached to a Zeiss Axio Imager M1 fluorescence microscope.

2.7. Cardiac function analysis

Echocardiography was performed using a Vevo 770 ultrasound system (Visualsonics, Toronto, ON, Canada) at day 5 after MI (n = 33) and 30 days after treatment (n = 9). Left ventricular ejection fraction (LVEF) and fractional area change (FAC) were quantified as previously described [27]. The echocardiographic data were acquired and analyzed in a blinded manner.

2.8. Morphometric and histological analysis

Animals were sacrificed for histological analysis at day 1 (CSCs n = 4 and CSCs-MPs n = 4), 7 (CSCs n = 4 and CSCs-MPs n = 4), 14 (CSCs n = 4 and CSCs-MPs n = 4) and 30 (CSCs n = 4 and CSCs-MPs n = 5) after treatment administration. Rats were anaesthetized, hearts were arrested in diastole (0.1 mM cadmium chloride Sigma-Aldrich) and perfusion-fixed for 15 min in 4% paraformaldehyde under physiologic pressure. After harvesting, the hearts were fixed overnight in 4% paraformaldehyde at 4 °C, sliced in three equally-sized blocks (apical, mid-ventricular, and basal), dehydrated in 70% ethanol (4 °C overnight), and embedded in paraffin. For histological analysis, 5 μm serial sections were prepared. Histological sections were immunostained and analyzed in a blinded manner.

2.8.1. Assessment of infarct size and cardiac fibrosis

Infarct size and tissue fibrosis were determined using Masson trichrome staining and Sirius Red staining in animals sacrificed 1-month post-treatment. For the Masson trichrome staining, 6 sections per heart were treated overnight in Bouin's solution, rinsed and stained with Weigert's hematoxylin for 5 min. They were then rinsed, stained with scarlet-acid fuchsin for 5 min and rinsed again. Then, slides were stained with phosphotungstic/phosphomolybdic, aniline blue, and 1% acetic acid for 5 min each. Slides were then rinsed and mounted in DPX. For the Sirius Red staininig, sections were deparaffinized and immersed for 30 min in 0.1% Fast Red (Sigma-Aldrich) diluted in a saturated solution of picric acid. They were then differentiated for 2 min in 0.01 N HCl (Sigma-Aldrich), dehydrated, and mounted in DPX. Infarct size and tissue fibrosis degree were assessed by quantifying 16 images from 8 serial heart sections, 30 μm apart. Images were analyzed using AnalySIS software and data were expressed as the percentage of the ischemic area *vs* total left ventricle area for infarct size and as fibrotic area (red) of the infarct zone *vs* total tissue area (percentage of collagen volume fraction: % CVF) for the fibrotic degree.

Periostin (POSTN) staining was performed in four different animals per group sacrificed 1-week post-treatment. Heart sections of 5 μm were washed in Tris-PBS (TPBS), non-specific IgG binding sites blocked with 8% goat serum (Dako), 1% BSA, and 0.1% Triton X-100 (Sigma-Aldrich) (SBT) and incubated overnight in rabbit anti-POSTN primary antibody (Abcam ab79946, 1:100) at 4 °C. The sections were then washed and incubated with Alexa 594-conjugated secondary antibody for 1 h before mounting. Negative controls were performed by incubating without the primary antibody. Cell nuclei were counterstained with 4′,6-diamidino-2-phenylindole (DAPI) (Sigma-Aldrich). All images were captured in a Zeiss Axio Imager M1 (Zeiss) fluorescent microscope.

The quantification of the POSTN$^+$ area was performed in stained sections from healthy and infarct tissue in four different animals per group sacrificed 1-week post-treatment. Between one and 5 pictures from infarct (IZ) and border zones (BZ) were taken from 3 different transversal sections per animal, located 150–200 μm from each other. The number of pixels of POSTN$^+$ (red) and DAPI$^+$ nuclei (blue) areas was determined using manual macros in Fiji software (1.46). For graphic representation, the percentage of the POSTN$^+$ area was calculated for each region.

2.8.2. Vascular density quantification

Tissue revascularization was evaluated in animals sacrificed 1 month post-treatment by quantifying the number of arterioles in the IZ and BZ using an anti-αSMA antibody conjugated to Cy3 (Sigma-Aldrich C6198, 1:500). Ten images from the border and ten from the infarct areas per section were randomly selected and counted from 7 serial sections from each animal. Images were acquired using an Axio Cam MR3 video camera at 20X connected to a Zeiss Axio Imager M1 microscope equipped with epifluorescence optics. Digital images were analyzed using MatLab® software platform (Mathworks Inc., Natick, MA, USA). Arteriolar density was expressed as the number of α-SMA-positive-vessels per mm^2.

2.9. Isolation of EVs secreted by CPCs cultured on biomimetic and non-biomimetic substrates

EVs from CPCs cultured on biomimetic and non-biomimetic flasks were isolated. The biomimetic functionalization of flasks was performed by coating T175 flasks with collagen type 1 of rat tail 3 mg/mL (Gibco-Invitrogen) and PDL (Sigma-Aldrich) (0.2 µg/cm^2 collagen and 0.3 µg/cm^2 PDL) at room temperature for 60 min. This biomimetic coating is similar to that used to prepare the biomimetic cell-adhesive microparticles. Flasks were subsequently rinsed twice with PBS and use immediately.

For EV isolation, 1.5 million CPCs were plated either in T175 biomimetic flasks or in non-coated flasks. After 48 h, cells were supplemented with the same medium described above (CSCs medium) without LIF and with 5% EV-depleted FBS. EV-depleted FBS was prepared by ultracentrifugation (25,000 rpm, 4 °C during 16 h) and filtration using a 0.22 μm syringe filter (Sartorius). A total of 180 mL of CPC-conditioned medium (CM) was collected at 24 h and 48 h and pooled together for EV isolation.

Two subpopulations enriched in different fractions of EVs, the 10K EVs and the 100K EVs, were isolated by several ultracentrifugation steps at 4 °C as described previously [28]. Briefly, CM was centrifuged twice at 3,400 rpm for 20 min at 4 °C (Heraeus, Megafuge 1.0 R, 7570F rotor) to remove detached cells and debris/apoptotic bodies. Supernatants were centrifuged at 8,200 rpm for 50 min (Optima LE-80k Ultracentrifuge, SW32 Ti rotor, Beckman Coulter) in conical tubes (Beckman Coulter). The pellet was rinsed in 2 mL of sterile PBS (Lonza), centrifuged at 10,000 rpm during 70 min at 4 °C and resuspended in 50 µL of sterile PBS to obtain the 10K EV fraction. The supernatant was filtered through a 0.20 μm syringe filter (28 mm PES membrane, Corning), pelleted by ultracentrifugation at 27,500 rpm for 190 min, rinsed in 25 mL of sterile PBS, ultracentrifuged again at 27,500 rpm for 190 min and resuspended in 50 µL of sterile PBS to obtain the 100K EV fraction. The manipulation of EVs was performed in a laminar flow hood to preserve sterility.

2.10. EV characterization

EV subpopulations were characterized using three different methods, following the statement from the International Society for Extracellular Vesicles [29]: Nanoparticle Tracking Analysis (NTA), Transmission Electron Microscopy (TEM), and western blot.

2.10.1. Nanoparticle tracking analysis of EVs

EV size distribution and quantification of vesicles were analyzed by NTA using a NanoSight NS3000 System (Malvern Instruments, UK). Samples were suspended in 0.22 μm pre-filtered PBS and dilutions were used to achieve a particle count between 30 and 100 particles/frame. Images were acquired for ninety seconds and the video was analyzed using a suitable particle detection threshold. Measurement of the diameter was performed on 3 independent experiments and showed as mode ± standard deviation (SD).

2.10.2. Transmission electron microscopy (TEM) of isolated EVs

Isolated EVs were diluted in PBS, loaded onto Formwar carbon-coated grids, fixed with 4% glutaraldehyde, contrasted with 2% uranyl methylcellulose and finally examined with an FEI Tecnai G2 Spirit transmission electron microscope. Images were acquired using a Morada CCD Camera (Olympus Soft Image Solutions GmbH).

2.10.3. Western blot of isolated EVs

EV total protein was quantified by BCA Protein Assay Kit (ThermoFisher Scientific) using an optimized version of the manufacturer protocol. Briefly, 10 µL of EVs were incubated 30 min at 4 °C with 6 µL of lysis buffer (1% Triton-X100, 0.1% SDS). Then, sterile water was added up to 60 µL, mixed with 600 µL of reagents A:B (1:50), and incubated at 60 °C during 60–90 min, together with a standard curve (0-to-1280 ng/well). The colour was determined using a SpectroStar-Nano (BMG Labtech) and data were analyzed using SpectroStar-Data analysis software (MARS). Afterwards, 1 µg of proteins was suspended in non-reducing Laemmli loading buffer and denatured at 100 °C for 5 min. Proteins were separated on 15% SDS-polyacrylamide gels and transferred to nitrocellulose membrane (Bio-Rad, 0.45 µm). Membranes were blocked using a Blocking Solution [5% non-fat dry milk powder and 0.05% Tween-20 in TBS buffer (1 mM Tris-HCl, 15 mM NaCl)] for 1 h at room temperature and incubated with the corresponding mouse or goat anti-rat primary antibody [specific for ALIX (1:1000), Calnexin (1:2500), or CD63 (1:5000) (SICGEN, Portugal)] in Blocking Solution overnight at 4 °C. After washing with TBS-0.05% Tween-20 solution, membranes were incubated for 2 h at room temperature with donkey anti-mouse or goat HRP-conjugated secondary antibody (Jackson ImmunoResearch Laboratories, Inc). Lumigen ECL Ultra (TMA-6) (Beckman Coulter) was applied for 5 min at room temperature for detection. ChemiDoc™ Imaging Systems (Bio-Rad) was used for image generation. Three technical replicates were performed.

2.11. Assessment of EV functionality

2.11.1. Isolation and culture of mouse cardiac fibroblasts (CFs)

Mouse cardiac interstitial cells (CICs) were obtained from 8 to 10 week old mice as previously described [30]. Briefly, after sacrifice, the thorax was opened and the heart was perfused with ice-cold PBS pH 7.6, atria were excised and tissues were placed in DMEM medium (Sigma-Aldrich) supplemented with 10% FBS (Hyclone, GE) on ice. Next, ventricles were minced using a sterile scalpel. Pieces of tissue were incubated in 125 µg/mL Liberase TH (Roche) in HBSS++ solution (Hanks balanced salt solution, Gibco) for 10 min at 37 °C in an orbital shaker. After the enzymatic incubation, the partially digested tissue was mechanically dissociated by slowly pipetting to reach a single cell suspension. The supernatant was filtered through a cell strainer to discard cardiomyocytes (40 μm, nylon; Falcon). The digestion was repeated with the sediment pieces and the supernatants were pooled together. The supernatant was centrifuged at 1500 rpm for 5 min and erythrocytes were removed using RBC lysis buffer (eBioscience). The total time for enzymatic digestion was 30 min. The final pellet was resuspended in complete medium [DMEM + 10% FBS + 1% P/S (Life Technology) + 1% L-Glu (Life Technology)] containing 10 ng/mL of bFGF (Peprotech) and plated in a 0.1% (w/v) gelatin-coated (Sigma-Aldrich) 6-well-plate (one heart per well). CFs were selected by attachment through washing the wells twice with PBS after overnight incubation and followed by a replacement of the complete medium plus 10 ng/mL of bFGF, lowering the concentration to 5 ng/mL (passage 1) and 2 ng/mL (passage 2) over time. After 24 h in passage 2, CFs were incubated in starving conditions (complete DMEM without FBS) overnight. Then they were supplemented with 100 µg/mL of specific fractions of EVs during 48 h.

2.11.2. RNA isolation and qPCR

Total RNA was isolated using TRIzol reagent (Ambion) according to the manufacturer's instructions. RNA purity (A260/A280 ratio ≥1.8) and concentration measured using the Nanodrop (Thermo Fisher). Total RNA was stored at −80 °C. Before cDNA preparation, genomic DNA was removed using a DNase treatment (Thermo Fisher). A total of 500 ng of RNA was converted into cDNA as per manufacturer's instructions (Takara). For each qPCR, the cDNA equivalent to 5 ng RNA was used. The qPCR reactions contained power SYBR green PCR master mix (Applied Biosystems) and an equimolar primer mix (0.8 μM). The amplification protocol consisted of 2 min at 50 °C, 10 min at 95 °C, followed by 40 cycles of 15 s at 95 °C, and 1 min at 60 °C, and completed with a standard melting curve protocol (15 s at 95 °C, 1 min at 60 °C and 15 s at 95 °C). The melting curve analysis (ViiA TM 7 Real-Time PCR system, Applied Biosystems) and size fractionation by agarose gel electrophoresis were used to confirm amplification of the expected products [31]. Target quantity (N_0) was obtained from the extracted raw data using *LinRegPCR* program [32]. Systematic differences induced by RT reactions in the observed expression levels per sample within tissue types as well as systematic differences between qPCR runs were removed using *Factor-qPCR* program [33].

Hptr1 and *Ppia* were selected as reference genes after a stability analysis using geNorm [34]. Primer sequences were designed using *primer3*, BLAST (NIH) and *oligo analyzer* (IDT) software, and they are summarized in Supplementary Table 1.

2.11.3. Wound healing (Scratch Assay) for cardiac fibroblast migration

Adult CFs from three mice in passage 2 were seeded in 24-well culture plates at a density of 1×10^4 cells/well. After 48 h, cells were subjected to starving conditions overnight. On the following day, cells were scraped in a straight line with a pipette tip. Cells were washed twice with PBS to remove debris and serum-free medium supplemented with different treatments (100 µg/mL of 100K EVs from CPCs cultured on biomimetic and non-biomimetic flasks) was added to the cells. The capacity of the cells to migrate into the denuded area was tracked using time-lapse microscopy *Cell Observer Z1* (Zeiss) for 48 h. The covered area was quantified using Fiji Software (1.46). Between 4 and 8 biological replicates were performed per condition.

2.11.4. Endothelial cell proliferation

A total of 1×10^4 MS1 cells (ATCC)/well in 96-well plates were seeded in complete medium (DMEM, 5% FBS, 1% P/S, 1% Sodium Pyruvate (Sigma-Aldrich)). After 24 h, cells were washed twice with PBS and incubated in starving conditions (Endothelial cell medium without FBS) with 30 mg/ml endothelial cell growth supplement (ECGS, Sigma-Aldrich) for 24 h. Cells were then incubated with or without 100 µg/mL of specific fractions of EVs in serum-free medium. Twenty-four hours after stimulation, cells were analyzed using the CellTiter 96 Aqueous One Solution Cell Proliferation Assay (MTS, Promega) and quantified with an ELISA reader at 490 nm.

2.12. Statistical analysis

All data are represented as mean ± standard error of the mean (SEM) unless mentioned differently. $POSTN^+$ area was represented as geometric mean ± SEM. For comparison between two groups, Student's *t*-test was used. Echocardiography outcomes and wound healing for cardiac fibroblast migration were analyzed by ANOVA, followed by post-hoc comparisons between time points by Tukey's multiple comparison test. qPCR results were analyzed using a non-parametric one-way analysis of variance with a Kruskal-Wallis post-hoc test. All statistical analyses were performed using GraphPad Prism (version 6.01), with the threshold for significance set at $P < 0.05$.

3. Results

3.1. Biomimetic MP preparation and in vitro *characterization*

Monodisperse spherical particles were successfully obtained using TROMS at high yield (80%). The mean particle size of the microcarriers measured by laser diffractometry was 4.8 ± 1.3 μm. MPs exhibited a negatively charged surface with a measured zeta potential of −14.3 mV, which is not adequate for cell adhesion. After particle surface modification, zeta potential measurements reflect that when PLGA MPs were coated with collagen and PDL, the resultant biomimetic microcarriers exhibited positive charges on the surface (+15.3 mV), this coating being essential to obtain a scaffold with cell-adhesive properties.

3.2. Efficient adhesion of CPCs to cell-adhesive MPs

After being coated with collagen and PDL, CPCs were seeded on the microcarriers (Fig. 1A). Cells attached easily to the MPs and almost all the cells adhered to the biomimetic microcarriers after 90 min at 37 °C in static culture (Fig. 1B and C).

3.3. In vivo *CPC survival in the ischemic myocardium*

Cell engraftment and survival was located and quantified in the host myocardium by immunofluorescence against GFP both in the acute and in the long-term stages post-treatment (24 h, 1 week, 2 weeks and 1-month post-treatment) (Fig. 1D and E). Twenty-four hours post-treatment, about 40% of the injected CPCs-MPs were found in the infarcted myocardium (CPCs-MPs = 39.01 ± 15.13% and CPCs = 29.03 ± 7.13%), indicating a 1.3 fold increase in cell retention during the initial stage of transplantation compared to the injection of CPCs alone. This effect was even more pronounced 1 and 2 weeks post-treatment, when cell survival increased 1.9 and 5.8 fold using MPs compared to the delivery of CPCs alone (1 week CPCs-MPs = 11.41 ± 6.19% and CPCs = 5.97 ± 4.98%) (2 weeks CPCs-MPs = 1.06 ± 0.68 and CPCs = 0.18 ± 0.15). Notably, one month after transplantation GFP^+ CPCs could also be detected (<1%) but only in the CPCs-MP treated group, suggesting that MPs also enhance the long-term survival of engrafted cells in the target ischemic myocardium. In addition, the proliferation of injected cells was analyzed by double staining for GFP/Ki67 at 7 days post-treatment. Remarkably, we found that transplanted cells were actively proliferating in both groups (CPCs = 9.3 ± 2.9% $Ki67^+/GFP^+$ and CPCs-MPs = 10.1 ± 2.0% $Ki67^+/GFP^+$) (Fig. 1F), indicating that the higher cell numbers observed in the CPCs-MP group could be attributed to the biomaterial and not to an increased proliferation rate. Overall, these results indicated that MPs support stem cell engraftment, increasing CPC survival in the infarcted rat hearts in both the acute-phase and the long term post-injection.

3.4. Effects of CPCs-MPs on heart function post-MI

Echocardiography at day 5 after MI showed that the initial infarct size was similar in both groups before treatment administration. LVEF was 38.83 ± 0.75% for CPCs and 38.76 ± 0.91% for CPCs-MPs. To evaluate the long-term effects of CPCs-MPs on cardiac function, echocardiography was performed 4 weeks after treatment administration (day 60 of the experiment/after MI) (Fig. 2A). LVEF in animals transplanted with CPCs improved at 4 weeks compared to pre-transplantation (CPCs day 5 after MI = 38.83 ± 0.75% *vs* CPCs 1 month post-treatment = 43.70 ± 2.12%). However, LVEF was significantly

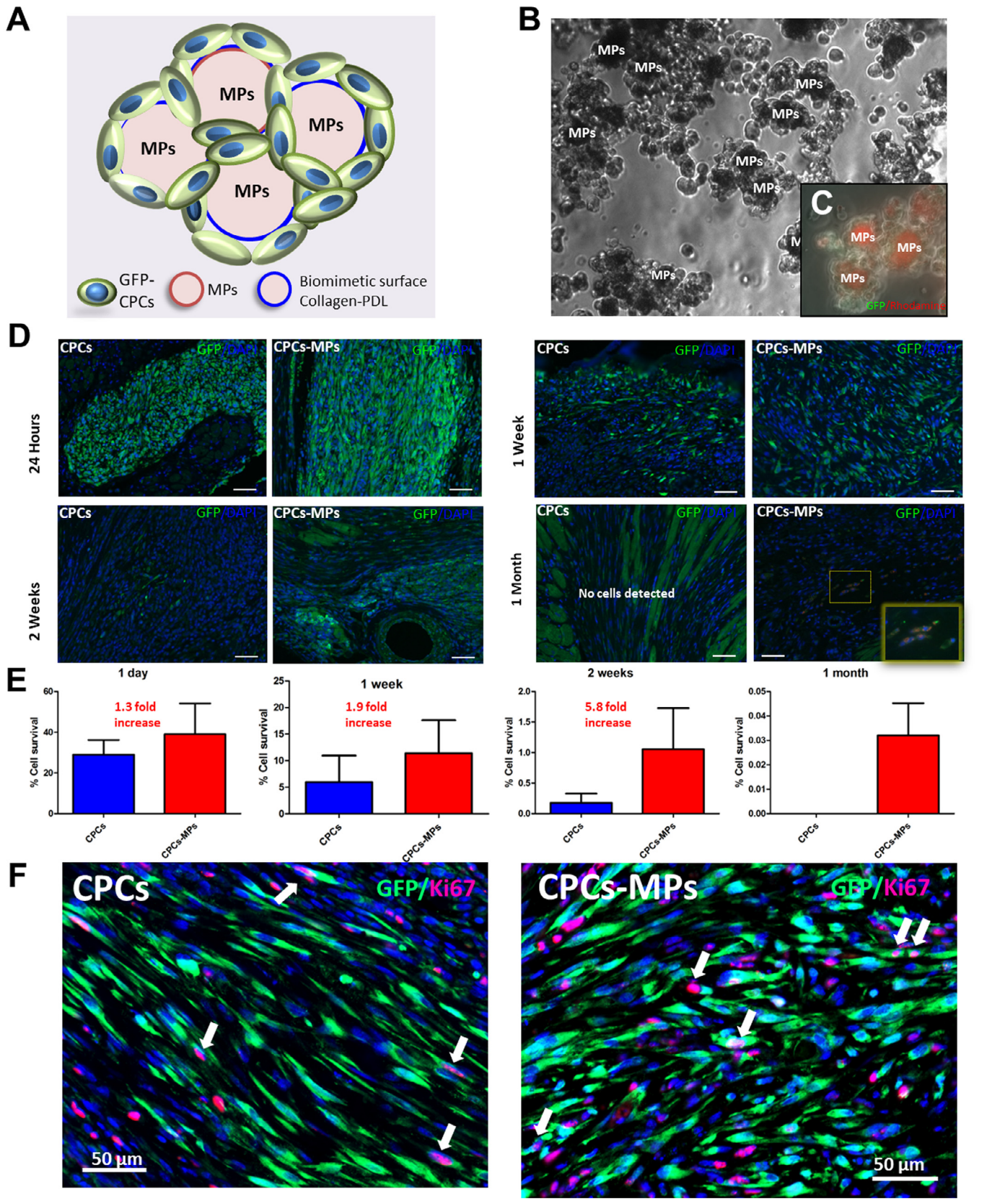

Fig. 1. CPCs-MPs promoted the survival of CPCs transplanted in the ischemic myocardium. (A) Schematic representation of the biomimetic and biodegradable microcarriers, which consists of injectable microparticulate scaffolds with a biomimetic surface of collagen and PDL that provide tridimensional support to CPCs. Bright-field (B) and fluorescent (C) images of the CPCs-MP complexes formed by 1×10^6 CPCs and 0.75 mg of biomimetic rhodamine loaded-MPs after 90 min of incubation. D) Representative immunofluorescent images of GFP staining (green, CPCs or CPCs-MPs) showing CPCs (green) engrafted in the infarcted myocardium at different time points after implantation (24 h, 1 week, 2 weeks and 1-month). Cell nuclei are stained with DAPI (blue). Scale bar: 50 µm. E) Quantification of cell survival in both groups at different time points. Data are expressed as mean ± SEM. F) Representative immunofluorescent images showing engrafted GFP (green)/Ki67 (red) double-positive CPCs 7 days after transplantation. Scale bar: 50 µm. (For interpretation of the references to color in this figure legend, the reader is referred to the web version of this article.)

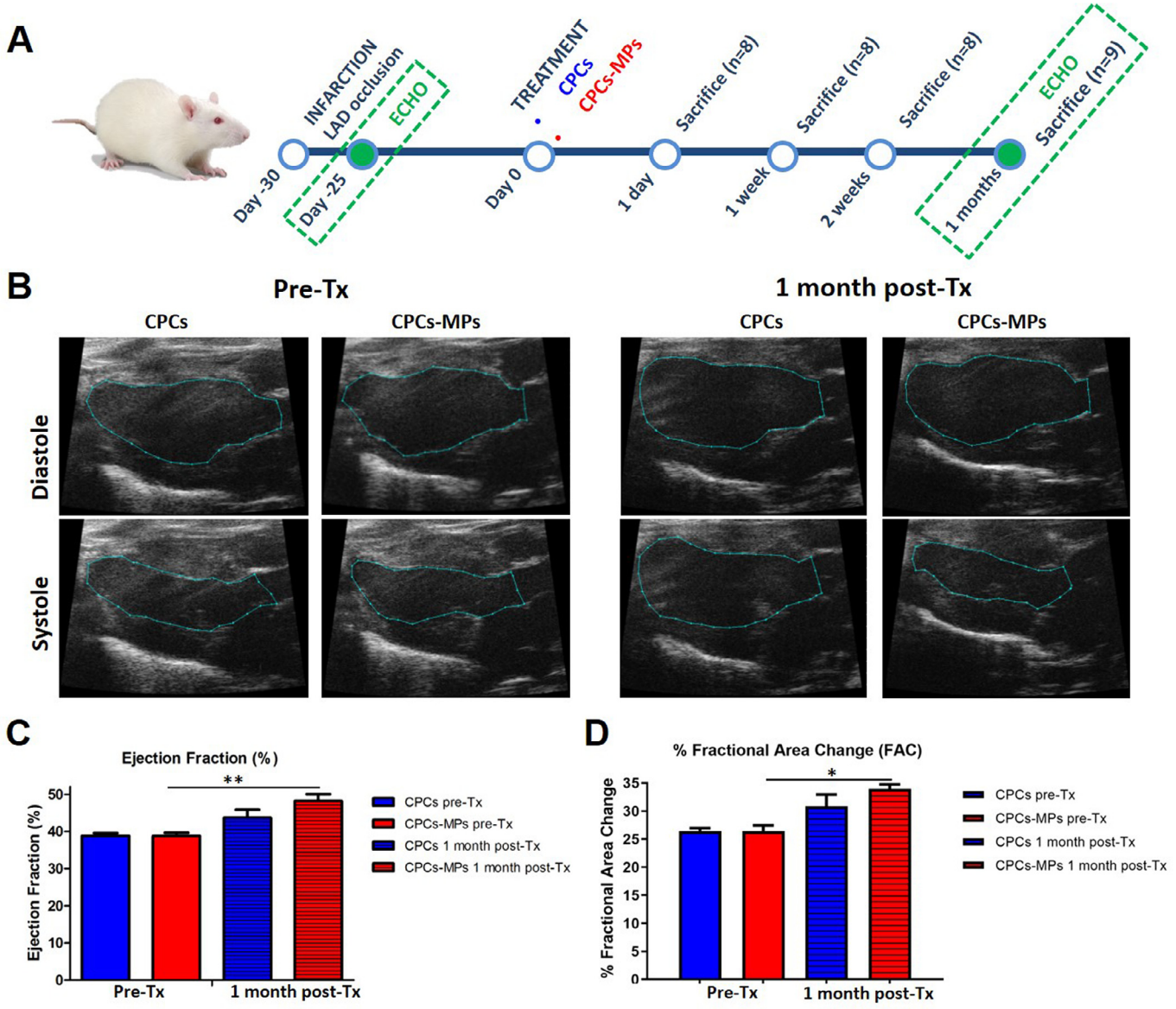

Fig. 2. Effects of CPCs-MPs on cardiac function. Cardiac function was evaluated 5 days after MI (pre-Tx) and 1 month after treatment (1-month post-Tx) by echocardiography. (A) Representative B-mode echocardiographic images in diastole and systole from a CPCs treated rat and a CPCs-MP treated rat. Ejection fraction (B) and fractional area change (FAC) (C) measured by echocardiography pre-treatment (pre-Tx) and 1-month post-treatment (1-month post-Tx) in animals treated with CPCs or with CPCs-MPs. Data are expressed as mean ± SEM. $^{*}P < 0.05$, $^{**}P < 0.01$.

higher only when CPCs were administered in combination with the microcarriers (CPCs-MP day 5 after MI = 38.76 ± 0.91% and CPCs-MP 1 month post-treatment = 48.2 ± 1.82% $P < 0.01$) (Fig. 2B). Similarly, FAC improved significantly only in those animals treated with the combination of CPCs and microcarriers (CPCs-MP day 5 after MI = 26.45 ± 1.00% and CPCs-MP 1 month post-treatment = 33.93 ± 0.82% $P < 0.05$). In CPC treated animals, an improvement in FAC was observed, although differences between pre and post-treatment were not statistically significant (CPCs day 5 after MI = 26.43 ± 0.53% and CPCs 1 month post-treatment = 30.84 ± 2.09%) (Fig. 2C). These data suggest that only the combination of CPCs with microcarriers improved cardiac function significantly.

3.5. CPCs-MPs improved adverse ventricular remodeling and angiogenesis in chronic MI

Next, the effect of CPCs-MPs on the infarct size was evaluated. Consistent with data on cardiac function, a larger area of healthy myocardium was found by Masson's Trichrome (Fig. 3A) and Sirius Red staining (Fig. 3B) in the CPCs-MP group. Moreover, infarct size was significantly smaller in animals treated with CPCs-MPs in comparison with CPCs-alone 1-month post-treatment (CPCs-MPs = 11.4 ± 0.5% and CPCs = 22.8 ± 2.3%, $P < 0.01$) (Fig. 3C), whereas LV thickness of the infarcted region was significantly greater in these animals (CPCs-MPs = 750.76 ± 64.94 μm and CPCs = 648.32 ± 69.83 μm, $P < 0.05$) (Fig. 3D).

Accordingly, collagen deposition was significantly attenuated in animals treated with CPCs-MPs when compared with the CPCs group 4 weeks post-implantation (CPCs-MPs = 38.4 ± 2.0% and CPCs = 45.9 ± 2.0% $P < 0.05$) (Fig. 4A).

POSTN is a secreted extracellular matrix component related to CF activation in the early phase of infarct healing [35]. Recent studies have described how the ablation of POSTN-expressing CFs in the subacute phase of MI results in reduced fibrosis and cardiac function without compromising scar stability [36]. Therefore, to further assess the anti-fibrotic effect of CPCs-MPs, the area covered by POSTN deposition was quantified in the BZ and IZ 1-week post-

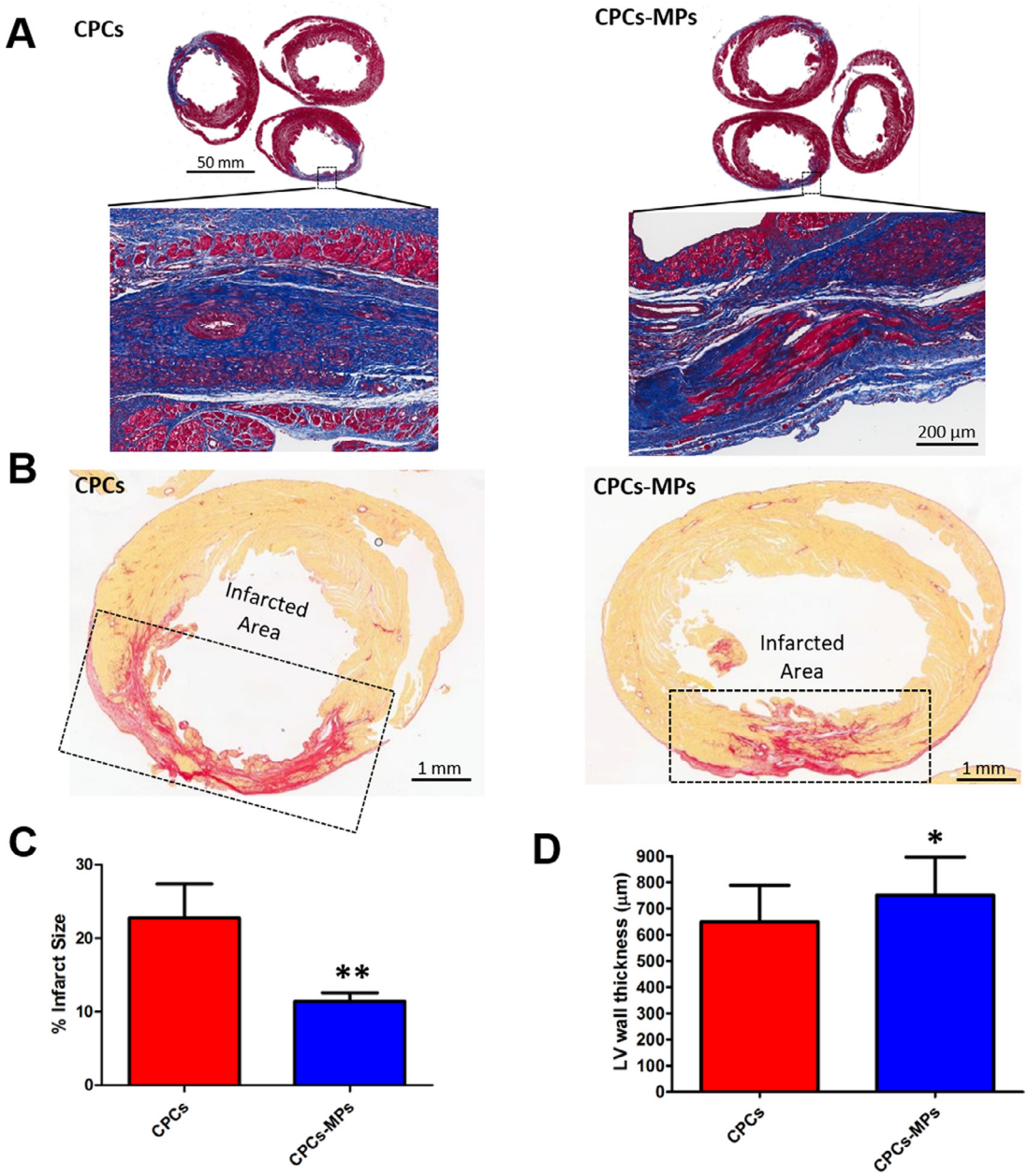

Fig. 3. CPCs-MPs reduced ventricular remodeling in the chronic phase of MI. (A) Representative Masson's trichrome-stained myocardial sections 1-month after treatment with CPCs or CPCs-MPs. Viable myocardium is identified by red color and scar tissue by blue color. Scale bar: 50 mm. The infarcted area in the box is magnified. Scale bar: 200 µm. (B) Representative scans/images of the infarcted heart sections stained with Sirius Red 1 month after treatment with CPCs or CPCs-MPs. Scale bar: 1 mm. Quantification of infarct size (C) and left ventricle wall thickness (D) comparing animals treated with CPCs and CPCs-MP 1 month post-treatment. Results are shown as mean ± SEM. $^{*}P < 0.05$, $^{**}P < 0.01$. (For interpretation of the references to color in this figure legend, the reader is referred to the web version of this article.)

treatment (5 weeks post-MI) as a measure of the area of fibrosis (Fig. 4A and B). POSTN deposits in the BZ were similar for CPCs and CPCs-MPs (CPCs = 8.98 ± 1.45% *vs* 9.07 ± 0.88%, respectively). Remarkably, POSTN deposits in the IZ showed a significant reduction of 30% in animals treated with CPCs-MPs compared to the CPCs-treated group (CPCs = 17.13 ± 1.49 *vs* CPCs-MPs = 11.64 ± 1.70% $P < 0.05$). These data suggest that administration of CPCs-MPs has an impact on the activity of activated cardiac fibroblast thus preventing adverse ventricular remodeling after chronic MI.

Vascularization is also a key process on cardiac repair after MI and therefore, the effect of CPCs-MPs on angiogenesis was next assessed by quantifying the number of arterioles/arteries (alpha-smooth muscle actin $[\alpha\text{-SMA}]^{+}$-coated vessels) in the heart ischemic areas. One month post-treatment the density of α-SMA^{+} vessels in the ischemic zone was significantly greater in animals treated with CPCs-MPs (79.13 ± 1.83 vessels/mm^2) than in those receiving CPCs alone (62.74 ± 1.91 vessels/mm^2) ($P < 0.001$) (Fig. 4C and D). Thus, an improvement on heart vascularization was observed after transplantation of CPCs combined with biomimetic microcarriers.

3.6. Culture of CPCs on a biomimetic environment with collagen and PDL affects cell morphology but not EV production

Our results on cell survival and engraftment on the ischemic myocardium suggest that paracrine factors are behind the therapeutic effects of CPCs, as previously described for these cells [8,11]. Therefore, we next explored whether culture of CPCs in

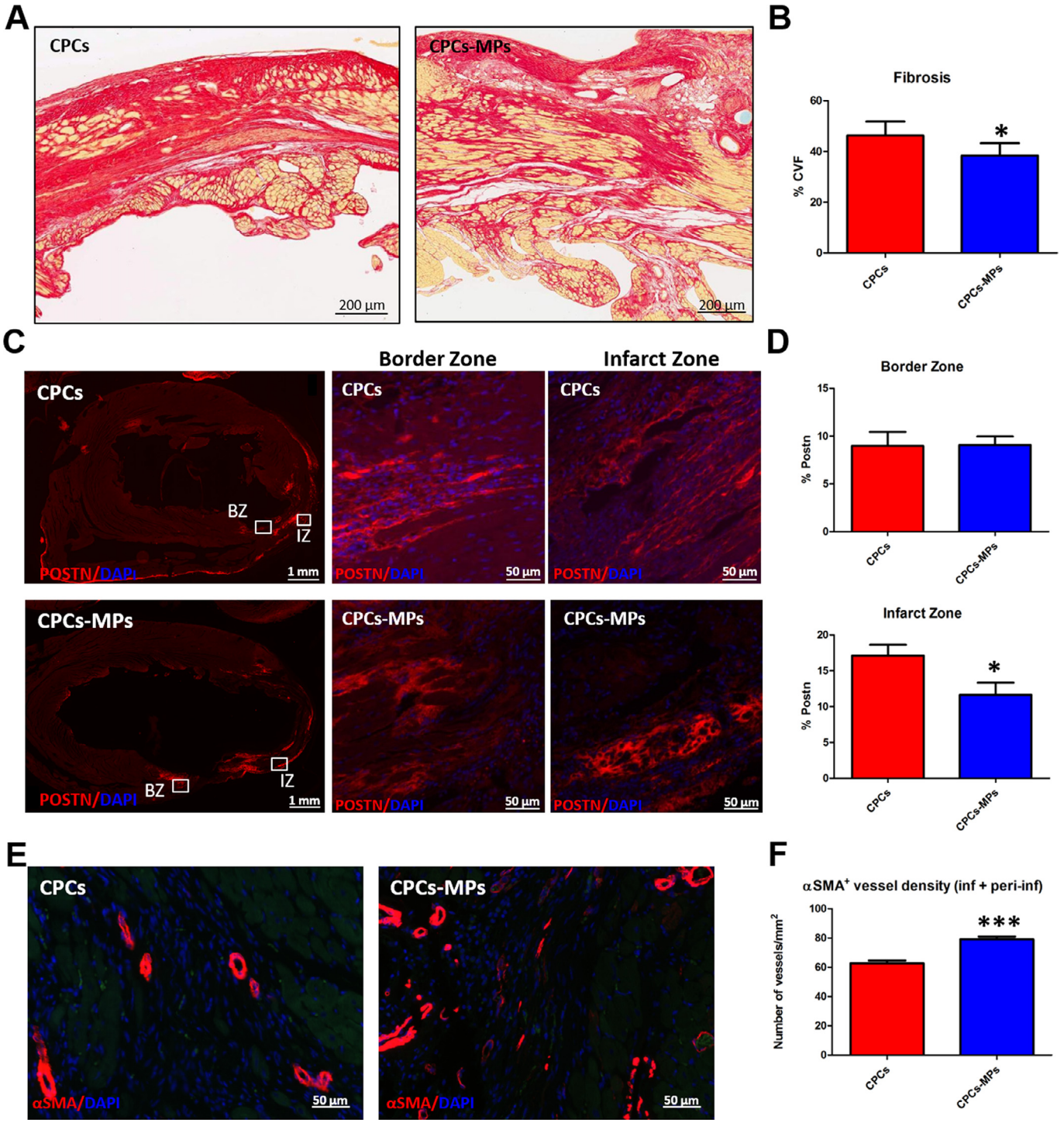

Fig. 4. CPCs-MPs reduced the deposition of collagen and periostin (POSTN) and improved angiogenesis in the chronic phase of MI. (A) Representative images and (B) quantification of collagen deposition expressed as the percentage of collagen volume fraction (% CVF) from CPCs and CPCs-MP treated groups after 1 month of treatment. Results are shown as mean ± SEM. Scale bar 100 µm. (C) Transversal sections of the infarcted hearts of rats treated with CPCs or CPCs-MP 1 week post treatment stained with POSTN (in red, left). Details of deposition of POSTN in the border (BZ, middle panel) and infarct zones (IZ, right). (D) Quantification of the area (%) of deposition of POSTN in both groups of animals 1 week after treatment in the BZ and IZ. Data are expressed as geometric mean ± SEM. (E) Representative images of α-SMA$^+$ vessels in the infarct zones of animals treated with CPCs or CPCs-MP one month after treatment. (F) Quantification of α-SMA$^+$ vessel density 1-month post-treatment in the ischemic zone of both groups of animals. Data are expressed as mean ± SEM. $^*P < 0.05$, $^{***}P < 0.001$. (For interpretation of the references to color in this figure legend, the reader is referred to the web version of this article.)

a biomimetic microenvironment could impact the CPC-release of EVs (10K and 100K EVs) (Fig. 5A). Culture of CPCs in collagen-PDL coated flasks induced changes in morphology with CPCs forming a number of spheroid bodies in contrast to non-coated ones, which grew as a monolayer (Fig. 5B). Next, 10K and 100K EVs isolated from CPCs cultured with or without coating were characterized [29]. TEM analysis of 10K and 100K EVs confirmed the presence of round-shaped vesicles surrounded by a bilayer membrane with heterogeneous sizes in both conditions (Fig. 5C). By NTA, the concentration of EVs related to the initial number of

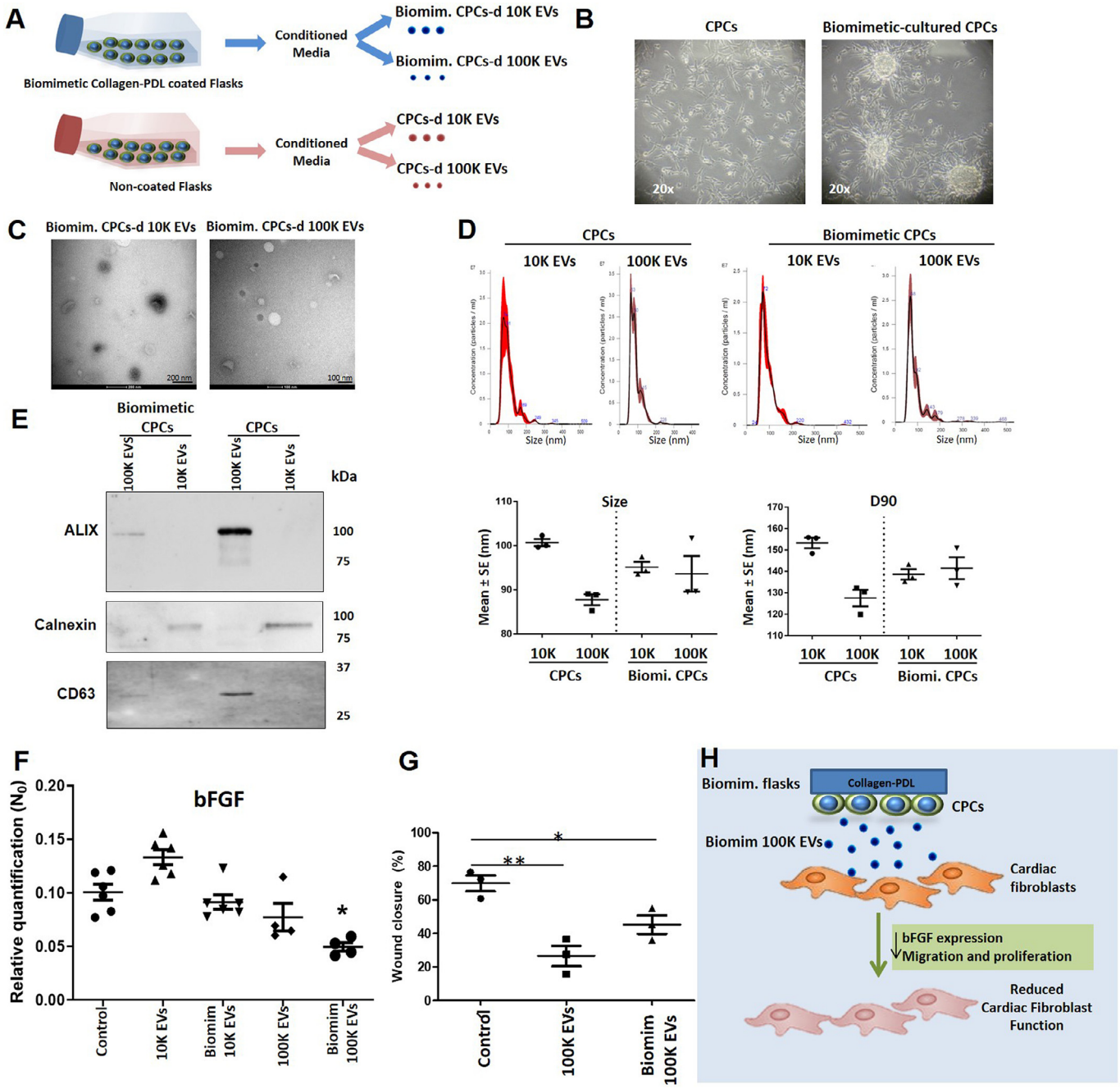

Fig. 5. EVs derived from CPCs cultured on collagen-PDL substrates display antifibrotic effects. (A) CPCs were plated either in biomimetic collagen-PDL flasks or in non-coated flasks. The CPC-conditioned medium was collected at 24 h and 48 h and pooled together for EV isolation. (B) Representative images of CPCs cultured on non-coated flasks (left) and CPCs cultured on biomimetic flasks (right). (C) Representative TEM images of biomimetic CPC-derived 10K EVs (left) and 100K EVs (right). Scale bar 200 nm (10K EVs) and 100 nm (100K EVs). (D) Graphical representation of the size distribution of both 10K and 100K EVs (above). Comparison of the mean size (left) and the D90 (right) of 10K *vs* 100K EVs isolated from CPCs or CPCs cultured under biomimetic conditions (below). (E) Representative western blots supporting the differences between 10K and 100K EVs isolated from CPCs and biomimetic CPCs for ALIX and CD63, both enriched on 100K EVs, and Calnexin, enriched in 10K EVs. (F) qPCR analysis of *bFgf* on mRNA of murine adult CFs cultured in normal conditions or in the presence of different populations of EVs (G) Wound healing assay. Quantification of wound closure percentage at 48 h from the initial wound area in the different groups. (H) Schematic illustration showing that 100K EVs derived from CPCs cultured on biomimetic substrates display antifibrotic effects.

cells did not change between conditions ($1.3 \times 10^9 \pm 11.8 \times 10^7$ particles/mL) indicating that culture on biomimetic substrate did not affect the concentration of EVs produced by CPCs. Interestingly, the size of the EV subpopulations produced in both culture conditions was very similar, ranging from 85 to 100 nm (10K EV size: 100.7 ± 0.8 nm D90: 153.26 ± 2.43 nm and 100K EV size: 87.76 ± 1.23 nm D90 127.56 ± 3.86 nm) (Biomim 10K EV size: 95.13 ± 1.2 nm D90: 138.600 ± 2.4 nm and Biomim 100K EV size: 93.63 ± 4 nm D90 141.46 ± 5.09 nm) (Fig. 5D). By western blot, the markers ALIX and CD63 were detected in both 100K EV and Biomimetic 100K EV-enriched populations. On the contrary, Calnexin was only present on the 10K preparations (Fig. 5E). Altogether, these analyses suggest that culture of CPCs on a biomimetic substrate does not affect EV production.

3.7. EVs derived from CPCs cultured on biomimetic substrates display antifibrotic effects

To elucidate whether EVs from CPCs cultured on biomimetic substrates of collagen/PDL were actively involved in cardiac remodeling, we analyzed their biological effects on primary murine CFs and MS1 endothelial cells. Based on our *in vivo* data (Figs. 3 and 4), we first investigated the expression of antifibrotic and angiogenic molecules after treatment of CFs with specific subpopulations of EVs (10K and 100K). *In vitro* 100K EVs from CPCs cultured under biomimetic conditions induced a significant decrease in the expression of the pro-fibrotic molecule *bFgf* (Fig. 5F) with no effect on the expression of other factors such as *Sdf-1*, *Nrg1*β or *Vegf-*α (data not shown) [37]. Since biomimetic 100K EVs significantly affect *bFgf* expression, we then investigated if they also inhibit CF growth using a scratch assay. Significant inhibition of the wound closure was observed after 48 h of treatment with 100K EVs from CPCs, indicating that they were able to inhibit CF growth. No differences, however, were found between biomimetic and non-biomimetic 100K EV subpopulations (Control: 69.93 $\pm$ 4.72%; Biomim 100K EVs: 44.33 $\pm$ 5.64% $p < 0.05$ *vs* control; and 100K EVs: 26.6 $\pm$ 6.05% $p < 0.01$ *vs* control) (Fig. 5G). These results suggest that 100K EVs from CPCs can attenuate CF activation (Fig. 5H). Finally, the effect of EVs on the proliferation of endothelial cells was evaluated. We did not find a significant difference in MS1 proliferation after co-culture with or without both types of EVs, suggesting no effects of EVs on MS1 cell proliferation (data not shown). Taken together, these results highlight that the beneficial effect obtained *in vivo* could be partially mediated by CPC-derived EVs.

4. Discussion

In this study, we have developed a bioengineered strategy for cardiac repair using biomimetic microcarriers to maximize CPC therapeutic properties. To demonstrate the potential of this strategy, we first show that biomimetic MPs allow for higher CPCs retention within the infarcted area in a rat model of chronic MI. In consequence, cardiac function, ventricular remodeling and angiogenesis were greater when using CPCs-MPs. Based on these *in vivo* results, we next turned to *in vitro* assays to investigate the underlying mechanisms involved in this process. We demonstrate that EVs from CPCs are actively involved in cardiac remodeling and that they display antifibrotic effects. Overall, this strategy can improve current cell therapy strategies with CPCs, offering a promising vehicle to deliver CPCs to the infarcted heart.

One of the main issues hindering the clinical translation of CPC-based therapies is poor effective engraftment within the ischemic myocardium. Microcarriers have been established as multidisciplinary systems that are very useful in the bioengineering field. In recent years, there has been interest in the development of cell mimicking MPs formed with a core polymer particle containing stem cell-secreted factors and coated with stem cell membranes [38]. So far, studies suggest that these synthetic particles preserve viable myocardium and increase cardiac function in a similar way to cardiac stem cell therapy [38]. This platform can be used for cardiac repair but also for other tissues such as liver [39]. In a different approach, microcarriers can be used as a tool for cell therapy since they have a high surface area to volume ratio which offers excellent 3D structural stability and anchoring points for injected cells [22,40,41]. Previous studies proved that microcarriers of 60 µm with a biomimetic surface of fibronectin and PDL increase cardiac retention of adipose-derived stem cells favoring tissue integration in animal models of cardiac ischemia [42,43]. Similarly, earlier studies by our group demonstrated the success of using microcarriers presenting a biomimetic surface of collagen and PDL to enhance the survival of both adipose-derived stem cells [14,20] and human cardiomyocytes [21] in the ischemic heart. Going a step further, here we show that microcarriers of 5 µm presenting a biomimetic surface of collagen and PDL are an excellent vehicle for CPC delivery and engraftment. The biomimetic coating of collagen/PDL may facilitate cell adhesion to the MPs, leading to a greater percentage of cells that survive after implantation. Moreover, collagen type I represents a good choice for the biomimetic coating given that this protein is the major component of the cardiac extracellular matrix [44]. Additionally, 5 µm MPs exhibit good injectability through percutaneous cardiac catheters [19] and excellent myocardial retention, being present in the heart tissue for up to 3 months post-implantation [25,45]. All of these aspects facilitate CPC contact with the damaged tissue and support their regenerative role.

The studies that report effective long-term engraftment of CPCs combined with biomaterials under pathological conditions are very scarce [46,47], and there are no clinical trials with CPCs using biomaterials at present. In particular, Gaetani et al. report the survival of hCPCs delivered using a 3D-printed cardiac patch of hyaluronic acid/gelatin in a mouse model of MI one month after transplantation [46]. Similarly, enhanced survival was also observed when rCPCs were seeded onto IGF-1 modified self-assembling nanofiber hydrogel and administered in the infarcted heart in a rat MI model [47]. Unlike previous biomaterial strategies, biomimetic microcarriers can be administered more easily than cardiac patches or hydrogels in the border zone using minimally invasive catheters [19], which, from a clinical perspective, supports its use as cardiac delivery vehicles. Additionally, only a few studies evaluated stem cell therapy during the chronic phase of MI [48–52], and, even less use biomaterials [17], which, therefore, makes the clinical translation difficult. Following the recommendations of the European Society of Cardiology Working Group Cellular Biology of the Heart to improve the therapeutic application of cell-based therapies for cardiac regeneration and repair [53], our therapy was assessed in a clinically relevant model of chronic MI. In the approach we describe, CPCs-MPs were administered 4 weeks after MI, as this time point represents a clinically translatable opportunity for treating MI patients. As a consequence of the greater CPC retention in the infarcted myocardium, our tissue-engineered strategy improved cardiac function and significantly reduced the infarct size and collagen deposition in the chronic MI model [49], this effect not being from the biomimetic MPs as we have previously demonstrated [21]. Moreover, relevant to the present study and consistent with the antifibrotic effects of CPCs-MPs, we found a reduction in POSTN in the IZ of these animals. While this extracellular matrix protein has been related to CF activation in the early phase of infarct healing [35], recent studies have associated POSTN with the reduction of fibrosis and the improvement in cardiac function when suppressed in the sub-acute phase of MI [36].

Given the percentage of CPCs that survive 1 month post-treatment, the enhanced beneficial effects found in our study may be mediated by paracrine mechanisms rather than by cell engraftment and differentiation into new cardiac cells/muscular mass [8,11]. Paracrine factors can be directly released into the extracellular space by CPCs or encapsulated in EVs, where they are packed and protected by the lipid bilayer from degradation by nucleases and proteinases. Supporting the idea that a paracrine mechanism is sufficient to observe functional effects, post-infarction administration of CPC-derived EVs recapitulates the beneficial effects of their parental cells [13]. Moreover, the EV cargo reflects the activation state of parental cells [54] and they have been proposed as therapeutic agents or drug delivery systems in regenerative medicine per se, or modified to be enriched in specific molecules. Consequently, recent investigations report that EVs from cardiac stem/progenitor cells are important anti-fibrotic mediators [12,55].

One example is the work by Bracco-Gartner et al. that describes the paracrine inhibitory effects of CPC-derived EVs on CFs using a GelMA hydrogel loaded with human fetal CFs in a model of cardiac fibrosis [55]. Likewise, cardiosphere-derived EVs act via switching inert fibroblasts into beneficial fibroblasts able to improve cardiac function when locally injected in the intramyocardial border zone of a rat model of chronic MI [12]. To all of this must be added new advances in biomaterials, which underline the importance of mimicking the native environment to achieve a better reparative response [56–58]. Therefore, to better understand the antifibrotic mechanisms behind CPCs-MP therapy, we next isolate and characterize two different subpopulations of EVs from CPCs cultured on biomimetic and non-biomimetic substrates. The first remarkable aspect is that, although 10K and 100K EVs showed different expression of markers and biological functions on CFs, NTA analysis showed that their size was quite similar (around 90–100 nm) independently of the substrate used to culture the cells. This could indicate that CPCs secrete EVs that are very homogeneous in size. Second, and perhaps the most notable implication is that biomimetic 100K EVs decrease significantly the expression of *bFgf* in CFs and inhibit its migration, which suggests that they can attenuate fibroblast function *in vitro* [49]. Something similar was found *in vivo*, when the biomimetic CPCs-MPs decreased POSTN deposits by 30% and collagen content by 17% in the IZ in the chronic MI model, indicating that our approach may be beneficial to reverse adverse ventricular remodeling in the chronic phase of MI. Therefore, our data provide insights into the mechanism by which CPCs adhered to a biomimetic substrate can reduce adverse post-ischemic remodeling. The results of our study are specifically related to the co-culture of EVs and CFs in the restricted *in vitro* environment. Thus, future studies warrant understanding the biology of EVs in a more relevant MI scenario. Further elucidation of the cargo of biomimetic EVs would help to understand the functional differences found *in vitro* between 10K and 100K EVs. Finally, the importance of using materials that provide biochemical and physical signals that mimic the native cardiac environment is also evidenced in our work, which may help in the design of more effective tissue engineering strategies for cardiac repair.

In conclusion, we demonstrate the possibility of using biomimetic microcarriers to enhance the delivery of CPCs to the ischemic myocardium in a clinically relevant animal model of MI. Our novel bioengineered strategy improves cardiac function, reduces chronic cardiac remodeling and increases vasculogenesis through the paracrine signalling of CPCs, suggesting an important role of EVs in the therapeutic effects of these cells. Thus, this strategy could improve current cell therapy approaches with CPCs, offering a promising vehicle to deliver cardiovascular progenitors to the infarcted heart.

Data availability

All data analyzed during this study are included in this manuscript. Other raw data required to reproduce these findings are available from the corresponding author on request.

Declaration of Competing Interest

BS and IP were employees of Coretherapix, (part of the Tigenix-Takeda since July 2018). BS and IP are co-inventors of the patent: “Adult cardiac stem cell population”. Application number: US201414213868.

Acknowledgements

This work was supported by the FEDER/Ministry of Science and Innovation-State Research Agency/SAF2017-83734-R and funds from the ISCIII and co-financed by FEDER (PI19/00501), Red TERCEL RETIC RD16/0011/0005 and MINECO (Program RETOS Cardiomesh RTC-2016-4911-1), ERANET II (Nanoreheart AC15/00050), and EU’s H2020 Programme for research, technological development and demonstration under grant agreement BRAV∃-874827. Elisa Garbayo is supported by a FSE/Ministry of Science and Innovation-State Research Agency RYC2018-025897-I. Adrian Ruiz-Villalba is supported by the Spanish Ministry of Sciences and Innovations FSE/MINECO-AEI(IJCI-2016-30254), and the Spanish Ministerio de Ciencia, Innovación y Universidades (grant RTI2018-095410-BI00). We thank Filippo Roli and Elena Iglesias for technical support.

Supplementary materials

Supplementary material associated with this article can be found, in the online version, at doi:10.1016/j.actbio.2021.03.017.

References

[1] G.A. Roth, C. Johnson, A. Abajobir, F. Abd-Allah, S.F. Abera, G. Abyu, M. Ahmed, B. Aksut, T. Alam, K. Alam, F. Alla, N. Alvis-Guzman, S. Amrock, H. Ansari, J. Ärnlöv, H. Asayesh, T.M. Atey, L. Avila-Burgos, A. Awasthi, A. Banerjee, A. Barac, T. Bärnighausen, L. Barregard, N. Bedi, E. Belay Ketema, D. Bennett, G. Berhe, Z. Bhutta, S. Bitew, J. Carapetis, J.J. Carrero, D.C. Malta, C.A. Castañeda-Orjuela, J. Castillo-Rivas, F. Catalá-López, J.-Y. Choi, H. Christensen, M. Cirillo, L. Cooper, M. Criqui, D. Cundiff, A. Damasceno, L. Dandona, R. Dandona, K. Davletov, S. Dharmaratne, P. Dorairaj, M. Dubey, R. Ehrenkranz, M. El Sayed Zaki, E.J.A. Faraon, A. Esteghamati, T. Farid, M. Farvid, V. Feigin, E.L. Ding, G. Fowkes, T. Gebrehiwot, R. Gillum, A. Gold, P. Gona, R. Gupta, T.D. Habtewold, N. Hafezi-Nejad, T. Hailu, G.B. Hailu, G. Hankey, H.Y. Hassen, K.H. Abate, R. Havmoeller, S.I. Hay, M. Horino, P.J. Hotez, K. Jacobsen, S. James, M. Javanbakht, P. Jeemon, D. John, J. Jonas, Y. Kalkonde, C. Karimkhani, A. Kasaeian, Y. Khader, A. Khan, Y.-H. Khang, S. Khera, A.T. Khoja, J. Khubchandani, D. Kim, D. Kolte, S. Kosen, K.J. Krohn, G.A. Kumar, G.F. Kwan, D.K. Lal, A. Larsson, S. Linn, A. Lopez, P.A. Lotufo, H.M.A. El Razek, R. Malekzadeh, M. Mazidi, T. Meier, K.G. Meles, G. Mensah, A. Meretoja, H. Mezgebe, T. Miller, E. Mirrakhimov, S. Mohammed, A.E. Moran, K.I. Musa, J. Narula, B. Neal, F. Ngalesoni, G. Nguyen, C.M. Obermeyer, M. Owolabi, G. Patton, J. Pedro, D. Qato, M. Qorbani, K. Rahimi, R.K. Rai, S. Rawaf, A. Ribeiro, S. Safiri, J.A. Salomon, I. Santos, M. Santric Milicevic, B. Sartorius, A. Schutte, S. Sepanlou, M.A. Shaikh, M.-J. Shin, M. Shishehbor, H. Shore, D.A.S. Silva, E. Sobngwi, S. Stranges, S. Swaminathan, R. Tabarés-Seisdedos, N. Tadele Atnafu, F. Tesfay, J.S. Thakur, A. Thrift, R. Topor-Madry, T. Truelsen, S. Tyrovolas, K.N. Ukwaja, O. Uthman, T. Vasankari, V. Vlassov, S.E. Vollset, T. Wakayo, D. Watkins, R. Weintraub, A. Werdecker, R. Westerman, C.S. Wiysonge, C. Wolfe, A. Workicho, G. Xu, Y. Yano, P. Yip, N. Yonemoto, M. Younis, C. Yu, T. Vos, M. Naghavi, C. Murray, Global, regional, and national burden of cardiovascular diseases for 10 causes, 1990 to 2015, J. Am. Coll. Cardiol. 70 (2017) 1–25, doi:10.1016/j.jacc.2017.04.052.

[2] P. Menasché, Cell therapy trials for heart regeneration–lessons learned and future directions, Nat. Rev. Cardiol. 15 (2018) 659–671, doi:10.1038/s41569-018-0013-0.

[3] J.N. Tang, J. Cores, K. Huang, X.L. Cui, L. Luo, J.Y. Zhang, T.S. Li, L. Qian, K. Cheng, Concise review: is cardiac cell therapy dead? Embarrassing trial outcomes and new directions for the future, Stem Cells Transl. Med. 7 (2018) 354–359, doi:10.1002/sctm.17-0196.

[4] L. Grigorian Shamagian, R. Madonna, D. Taylor, A.M. Climent, F. Prosper, L. Bras-Rosario, A. Bayes-Genis, P. Ferdinandy, F. Fernández-Avilés, J.C. Izpisua Belmonte, V. Fuster, R. Bolli, Perspectives on directions and priorities for future preclinical studies in regenerative medicine, Circ. Res. 124 (2019) 938–951, doi:10.1161/CIRCRESAHA.118.313795.

[5] R.R. Makkar, R.R. Smith, K. Cheng, K. Malliaras, L.E. Thomson, D. Berman, L.S. Czer, L. Marbán, A. Mendizabal, P.V Johnston, S.D. Russell, K.H. Schuleri, A.C. Lardo, G. Gerstenblith, E. Marbán, Intracoronary cardiosphere-derived cells for heart regeneration after myocardial infarction (CADUCEUS): a prospective, randomised phase 1 trial, Lancet (London, England) 379 (2012) 895–904, doi:10.1016/S0140-6736(12)60195-0.

[6] M.H. Yacoub, J. Terrovitis, CADUCEUS, SCIPIO, ALCADIA: cell therapy trials using cardiac-derived cells for patients with post myocardial infarction LV dysfunction, still evolving, Glob. Cardiol. Sci. Pract. (2013) 5–8 2013, doi:10.5339/gcsp.2013.3.

[7] N. Takehara, Y. Tsutsumi, K. Tateishi, T. Ogata, H. Tanaka, T. Ueyama, T. Takahashi, T. Takamatsu, M. Fukushima, M. Komeda, M. Yamagishi, H. Yaku, Y. Tabata, H. Matsubara, H. Oh, Controlled delivery of basic fibroblast growth factor promotes human cardiosphere-derived cell engraftment to enhance cardiac repair for chronic myocardial infarction, J. Am. Coll. Cardiol. 52 (2008) 1858–1865, doi:10.1016/j.jacc.2008.06.052.

[8] N. Witman, C. Zhou, N. Grote Beverborg, M. Sahara, K.R. Chien, Cardiac progenitors and paracrine mediators in cardiogenesis and heart regeneration, Semin. Cell Dev. Biol. 100 (2020) 29–51, doi:10.1016/j.semcdb.2019.10.011.

[9] A.G.-E. Ibrahim, K. Cheng, E. Marbán, Exosomes as critical agents of cardiac regeneration triggered by cell therapy, Stem Cell Rep. 2 (2014) 606–619, doi:10.1016/j.stemcr.2014.04.006.
[10] R. Shah, T. Patel, J.E. Freedman, Circulating extracellular vesicles in human disease, N. Engl. J. Med. 379 (2018) 958–966, doi:10.1056/NEJMra1704286.
[11] J.A. Maring, K. Lodder, E. Mol, V. Verhage, K.C. Wiesmeijer, C.K.E. Dingenouts, A.T. Moerkamp, J.C. Deddens, P. Vader, A.M. Smits, J.P.G. Sluijter, M.J. Goumans, Cardiac progenitor cell–derived extracellular vesicles reduce infarct size and associate with increased cardiovascular cell proliferation, J. Cardiovasc. Transl. Res. 12 (2019) 5–17, doi:10.1007/s12265-018-9842-9.
[12] E. Tseliou, J. Fouad, H. Reich, L. Slipczuk, G. de Couto, M. Aminzadeh, R. Middleton, J. Valle, L. Weixin, E. Marbán, Fibroblasts rendered antifibrotic, antiapoptotic, and angiogenic by priming with cardiosphere-derived extracellular membrane vesicles, J. Am. Coll. Cardiol. 66 (2015) 599–611, doi:10.1016/j.jacc.2015.05.068.
[13] A. Kervadec, V. Bellamy, N. El Harane, L. Arakélian, V. Vanneaux, I. Cacciapuoti, H. Nemetalla, M.C. Périer, H.D. Toeg, A. Richart, M. Lemitre, M. Yin, X. Loyer, J. Larghero, A. Hagège, M. Ruel, C.M. Boulanger, J.S. Silvestre, P. Menasché, N.K.E. Renault, Cardiovascular progenitor-derived extracellular vesicles recapitulate the beneficial effects of their parent cells in the treatment of chronic heart failure, J. Hear. Lung Transplant. 35 (2016) 795–807, doi:10.1016/j.healun.2016.01.013.
[14] P. Díaz-Herráez, L. Saludas, S. Pascual-Gil, T. Simón-Yarza, G. Abizanda, F. Prósper, E. Garbayo, M.J. Blanco-Prieto, Transplantation of adipose-derived stem cells combined with neuregulin-microparticles promotes efficient cardiac repair in a rat myocardial infarction model, J. Control. Release 249 (2017) 23–31, doi:10.1016/j.jconrel.2017.01.026.
[15] S. Pascual-Gil, E. Garbayo, P. Díaz-Herráez, F. Prosper, M.J. Blanco-Prieto, Heart regeneration after myocardial infarction using synthetic biomaterials, J. Control. Release (2015) 203, doi:10.1016/j.jconrel.2015.02.009.
[16] L. Saludas, S. Pascual-Gil, F. Prósper, E. Garbayo, M. Blanco-Prieto, Hydrogel based approaches for cardiac tissue engineering, Int. J. Pharm. 523 (2017), doi:10.1016/j.ijpharm.2016.10.061.
[17] M. Araña, J.J. Gavira, E. Peña, A. González, G. Abizanda, M. Cilla, M.M. Pérez, E. Albiasu, N. Aguado, M. Casado, B. López, S. González, M. Soriano, C. Moreno, J. Merino, J.M. García-Verdugo, J. Díez, M. Doblaré, B. Pelacho, F. Prosper, Epicardial delivery of collagen patches with adipose-derived stem cells in rat and minipig models of chronic myocardial infarction, Biomaterials 35 (2014) 143–51, doi:10.1016/j.biomaterials.2013.09.083.
[18] E. Garbayo, E. Ansorena, H. Lana, M. del M. Carmona-Abellan, I. Marcilla, J.L. Lanciego, M.R. Luquin, M.J. Blanco-Prieto, Brain delivery of microencapsulated GDNF induces functional and structural recovery in parkinsonian monkeys, Biomaterials 110 (2016) 11–23, doi:10.1016/j.biomaterials.2016.09.015.
[19] E. Garbayo, J.J. Gavira, M.G. De Yebenes, B. Pelacho, G. Abizanda, H. Lana, M.J. Blanco-Prieto, F. Prosper, Catheter-based intramyocardial injection of FGF1 or NRG1-loaded MPs improves cardiac function in a preclinical model of ischemia-reperfusion, Sci. Rep. 6 (2016), doi:10.1038/srep25932.
[20] P. Díaz-Herráez, E. Garbayo, T. Simón-Yarza, F.R. Formiga, F. Prosper, M.J. Blanco-Prieto, Adipose-derived stem cells combined with Neuregulin-1 delivery systems for heart tissue engineering, Eur. J. Pharm. Biopharm. 85 (2013), doi:10.1016/j.ejpb.2013.03.022.
[21] L. Saludas, E. Garbayo, M. Mazo, B. Pelacho, G. Abizanda, O. Iglesias Garcia, A. Raya, F. Prosper, M.J. Blanco-prieto, Long-term engraftment of human cardiomyocytes combined with biodegradable microparticles induces heart repair, J. Pharmacol. Exp. Ther. (2019) jpet.118.256065, doi:10.1124/jpet.118.256065.
[22] M.D. Neto, M.B. Oliveira, J.F. Mano, Microparticles in Contact with cells: from carriers to multifunctional tissue modulators, Trends Biotechnol. (2019), doi:10.1016/j.tibtech.2019.02.008.
[23] F. Fernández-Avilés, R. Sanz-Ruiz, J. Bogaert, A.C. Plasencia, I. Gilaberte, A. Belmans, M.E. Fernández-Santos, D. Charron, M. Mulet, R. Yotti, I. Palacios, M. Luque, R. Sádaba, J.A.S. Román, M. Larman, P.L. Sánchez, J. Sanchís, M.F. Jiménez, P. Claus, R. Al-Daccak, E. Lombardo, J.L. Abad, O. Delarosa, L. Corcóstegui, J. Bermejo, S. Janssens, Safety and efficacy of intracoronary infusion of allogeneic human cardiac stem cells in patients with st-segment elevation myocardial infarction and left ventricular dysfunction a multicenter randomized, double-blind, and placebo-controlled clinical trial, Circ. Res. 123 (2018) 579–589, doi:10.1161/CIRCRESAHA.118.312823.
[24] V. Crisostomo, C. Baez-Diaz, J. Maestre, M. Garcia-Lindo, F. Sun, J.G. Casado, R. Blazquez, J.L. Abad, I. Palacios, L. Rodriguez-Borlado, F.M. Sanchez-Margallo, Delayed administration of allogeneic cardiac stem cell therapy for acute myocardial infarction could ameliorate adverse remodeling: experimental study in swine, J. Transl. Med. 13 (2015) 156, doi:10.1186/s12967-015-0512-2.
[25] S. Pascual-Gil, T. Simón-Yarza, E. Garbayo, F. Prosper, M.J. Blanco-Prieto, Tracking the in vivo release of bioactive NRG from PLGA and PEG-PLGA microparticles in infarcted hearts, J. Control. Release 220 (2015) 388–396, doi:10.1016/j.jconrel.2015.10.058.
[26] F.R. Formiga, B. Pelacho, E. Garbayo, I. Imbuluzqueta, P. Díaz-Herráez, G. Abizanda, J.J. Gavira, T. Simón-Yarza, E. Albiasu, E. Tamayo, F. Prósper, M.J. Blanco-Prieto, Controlled delivery of fibroblast growth factor-1 and neuregulin-1 from biodegradable microparticles promotes cardiac repair in a rat myocardial infarction model through activation of endogenous regeneration, J. Control. Release (2013), doi:10.1016/j.jconrel.2013.10.034.
[27] C. Benavides-Vallve, D. Corbacho, O. Iglesias-Garcia, B. Pelacho, E. Albiasu, S. Castaño, A. Muñoz-Barrutia, F. Prosper, C. Ortiz-de-Solorzano, New strategies for echocardiographic evaluation of left ventricular function in a mouse model of long-term myocardial infarction, PLoS One 7 (2012) e41691, doi:10.1371/journal.pone.0041691.
[28] C. Théry, S. Amigorena, G. Raposo, A. Clayton, Isolation and characterization of exosomes from cell culture supernatants and biological fluids, Curr. Protoc. Cell Biol. 30 (2006) 3.22.1-3.22.29, doi:10.1002/0471143030.cb0322s30.
[29] J. Lötvall, A.F. Hill, F. Hochberg, E.I. Buzás, D. Di Vizio, C. Gardiner, Y.S. Gho, I.V Kurochkin, S. Mathivanan, P. Quesenberry, S. Sahoo, H. Tahara, M.H. Wauben, K.W. Witwer, C. Théry, Minimal experimental requirements for definition of extracellular vesicles and their functions: a position statement from the International Society for Extracellular Vesicles, J. Extracell. Vesicles 3 (2014) 26913, doi:10.3402/jev.v3.26913.
[30] A. Ruiz-Villalba, A.M. Simón, C. Pogontke, M.I. Castillo, G. Abizanda, B. Pelacho, R. Sánchez-Domínguez, J.C. Segovia, F. Prósper, J.M. Pérez-Pomares, Interacting resident epicardium-derived fibroblasts and recruited bone marrow cells form myocardial infarction scar, J. Am. Coll. Cardiol. 65 (2015) 2057–2066, doi:10.1016/j.jacc.2015.03.520.
[31] A. Ruiz-Villalba, E. van Pelt-Verkuil, Q.D. Gunst, J.M. Ruijter, M.J. van den Hoff, Amplification of nonspecific products in quantitative polymerase chain reactions (qPCR), Biomol. Detect. Quantif. 14 (2017) 7–18, doi:10.1016/j.bdq.2017.10.001.
[32] J.M. Ruijter, C. Ramakers, W.M.H. Hoogaars, Y. Karlen, O. Bakker, M.J.B. van den Hoff, A.F.M. Moorman, Amplification efficiency: linking baseline and bias in the analysis of quantitative PCR data, Nucl. Acids Res. 37 (2009) e45, doi:10.1093/nar/gkp045.
[33] J.M. Ruijter, A. Ruiz Villalba, J. Hellemans, A. Untergasser, M.J.B. van den Hoff, Removal of between-run variation in a multi-plate qPCR experiment, Biomol. Detect. Quantif. 5 (2015) 10–14, doi:10.1016/j.bdq.2015.07.001.
[34] J. Vandesompele, K. De Preter, F. Pattyn, B. Poppe, N. Van Roy, A. De Paepe, F. Speleman, Accurate normalization of real-time quantitative RT-PCR data by geometric averaging of multiple internal control genes, Genome Biol. 3 (2002) research0034.1, doi:10.1186/gb-2002-3-7-research0034.
[35] T. Oka, J. Xu, R.A. Kaiser, J. Melendez, M. Hambleton, M.A. Sargent, A. Lorts, E.W. Brunskill, G.W. Dorn, S.J. Conway, B.J. Aronow, J. Robbins, J.D. Molkentin, Genetic Manipulation of periostin expression reveals a role in cardiac hypertrophy and ventricular remodeling, Circ. Res. 101 (2007) 313–321, doi:10.1161/CIRCRESAHA.107.149047.
[36] H. Kaur, M. Takefuji, C.Y. Ngai, J. Carvalho, J. Bayer, A. Wietelmann, A. Poetsch, S. Hoelper, S.J. Conway, H. Möllmann, M. Looso, C. Troidl, S. Offermanns, N. Wettschureck, Targeted ablation of periostin-expressing activated fibroblasts prevents adverse cardiac remodeling in mice, Circ. Res. 118 (2016) 1906–1917, doi:10.1161/CIRCRESAHA.116.308643.
[37] M. Kanada, M.H. Bachmann, J.W. Hardy, D.O. Frimannson, L. Bronsart, A. Wang, M.D. Sylvester, T.L. Schmidt, R.L. Kaspar, M.J. Butte, A.C. Matin, C.H. Contag, Differential fates of biomolecules delivered to target cells via extracellular vesicles, Proc. Natl. Acad. Sci. USA 112 (2015) E1433–E1442, doi:10.1073/pnas.1418401112.
[38] J. Tang, D. Shen, T.G. Caranasos, Z. Wang, A.C. Vandergriff, T.A. Allen, M.T. Hensley, P.U. Dinh, J. Cores, T.S. Li, J. Zhang, Q. Kan, K. Cheng, Therapeutic microparticles functionalized with biomimetic cardiac stem cell membranes and secretome, Nat. Commun. 8 (2017), doi:10.1038/ncomms13724.
[39] H. Liang, K. Huang, T. Su, Z. Li, S. Hu, P.U. Dinh, E.A. Wrona, C. Shao, L. Qiao, A.C. Vandergriff, M.T. Hensley, J. Cores, T. Allen, H. Zhang, Q. Zeng, J. Xing, D.O. Freytes, D. Shen, Z. Yu, K. Cheng, Mesenchymal stem cell/red blood cell-inspired nanoparticle therapy in mice with carbon tetrachloride-induced acute liver failure, ACS Nano 12 (2018) 6536–6544, doi:10.1021/acsnano.8b00553.
[40] M.B. Oliveira, J.F. Mano, Polymer-based microparticles in tissue engineering and regenerative medicine, Biotechnol. Prog. 27 (2011) 897–912, doi:10.1002/btpr.618.
[41] C.A. Custódio, V.E. Santo, M.B. Oliveira, M.E. Gomes, R.L. Reis, J.F. Mano, Functionalized microparticles producing scaffolds in combination with cells, Adv. Funct. Mater. 24 (2014) 1391–1400, doi:10.1002/adfm.201301516.
[42] M. Savi, L. Bocchi, E. Fiumana, J.-P. Karam, C. Frati, F. Bonafé, S. Cavalli, P.G. Morselli, C. Guarnieri, C.M. Caldarera, C. Muscari, C.N. Montero-Menei, D. Stilli, F. Quaini, E. Musso, Enhanced engraftment and repairing ability of human adipose-derived stem cells, conveyed by pharmacologically active microcarriers continuously releasing HGF and IGF-1, in healing myocardial infarction in rats, J. Biomed. Mater. Res. A 103 (2015) 3012–25, doi:10.1002/jbm.a.35442.
[43] R. Madonna, L. Petrov, M.A. Teberino, L. Manzoli, J.-P. Karam, F.V. Renna, P. Ferdinandy, C.N. Montero-Menei, S. Ylä-Herttuala, R. De Caterina, Transplantation of adipose tissue mesenchymal cells conjugated with VEGF-releasing microcarriers promotes repair in murine myocardial infarction, Cardiovasc. Res. 108 (2015) 39–49, doi:10.1093/cvr/cvv197.
[44] C. Jourdan-LeSaux, J. Zhang, M.L. Lindsey, Extracellular matrix roles during cardiac repair, Life Sci. 87 (2010) 391–400, doi:10.1016/j.lfs.2010.07.010.
[45] F.R. Formiga, E. Garbayo, P. Díaz-Herráez, G. Abizanda, T. Simón-Yarza, E. Tamayo, F. Prósper, M.J. Blanco-Prieto, Biodegradation and heart retention of polymeric microparticles in a rat model of myocardial ischemia, Eur. J. Pharm. Biopharm. 85 (2013), doi:10.1016/j.ejpb.2013.02.017.
[46] R. Gaetani, D.A.M. Feyen, V. Verhage, R. Slaats, E. Messina, K.L. Christman, A. Giacomello, P.A.F.M. Doevendans, J.P.G. Sluijter, Epicardial application of cardiac progenitor cells in a 3D-printed gelatin/hyaluronic acid patch preserves cardiac function after myocardial infarction, Biomaterials 61 (2015) 339–348, doi:10.1016/j.biomaterials.2015.05.005.

[47] M.E. Padin-Iruegas, Y. Misao, M.E. Davis, V.F.M. Segers, G. Esposito, T. Tokunou, K. Urbanek, T. Hosoda, M. Rota, P. Anversa, A. Leri, R.T. Lee, J. Kajstura, Cardiac progenitor cells and biotinylated insulin-like growth factor-1 nanofibers improve endogenous and exogenous myocardial regeneration after infarction, Circulation 120 (2009) 876–87, doi:10.1161/CIRCULATIONAHA.109.852285.

[48] J.C. Deddens, D.A. Feyen, P.P. Zwetsloot, M.A. Brans, S. Siddiqi, L.W. Van Laake, P.A. Doevendans, J.P. Sluijter, Targeting chronic cardiac remodeling with cardiac progenitor cells in a murine model of ischemia/reperfusion injury, PLoS One (2017) 12, doi:10.1371/journal.pone.0173657.

[49] E. Tseliou, H. Reich, G. de Couto, J. Terrovitis, B. Sun, W. Liu, E. Marbán, Cardiospheres reverse adverse remodeling in chronic rat myocardial infarction: roles of soluble endoglin and Tgf-β signaling, Basic Res. Cardiol. 109 (2014), doi:10.1007/s00395-014-0443-8.

[50] X.L. Tang, G. Rokosh, S.K. Sanganalmath, F. Yuan, H. Sato, J. Mu, S. Dai, C. Li, N. Chen, Y. Peng, B. Dawn, G. Hunt, A. Leri, J. Kajstura, S. Tiwari, G. Shirk, P. Anversa, R. Bolli, Intracoronary administration of cardiac progenitor cells alleviates left ventricular dysfunction in rats with a 30-day-old infarction, Circulation 121 (2010) 293–305, doi:10.1161/CIRCULATIONAHA.109.871905.

[51] M. Rota, M.E. Padin-Iruegas, Y. Misao, A. De Angelis, S. Maestroni, J. Ferreira-Martins, E. Fiumana, R. Rastaldo, M.L. Arcarese, T.S. Mitchell, A. Boni, R. Bolli, K. Urbanek, T. Hosoda, P. Anversa, A. Leri, J. Kajstura, Local activation or implantation of cardiac progenitor cells rescues scarred infarcted myocardium improving cardiac function, Circ. Res. 103 (2008) 107–116, doi:10.1161/CIRCRESAHA.108.178525.

[52] N. Latham, B. Ye, R. Jackson, B.K. Lam, D. Kuraitis, M. Ruel, E.J. Suuronen, D.J. Stewart, D.R. Davis, Human blood and cardiac stem cells synergize to enhance cardiac repair when cotransplanted into ischemic myocardium, Circulation 128 (2013), doi:10.1161/CIRCULATIONAHA.112.000374.

[53] R. Madonna, L.W. Van Laake, S.M. Davidson, F.B. Engel, J.H. Derek, S. Lecour, J. Leor, C. Perrino, R. Schulz, K. Ytrehus, U. Landmesser, C.L. Mummery, S. Janssens, J. Willerson, T. Eschenhagen, P. Ferdinandy, J.P.G. Sluijter, Position paper of the european society of cardiology working group cellular biology of the heart: cell-based therapies for myocardial repair and regeneration in ischemic heart disease and heart failure, Eur. Hear. J. 37 (2016) 1789–1798, doi:10.1093/eurheartj/ehw113.

[54] L. Qiao, S. Hu, S. Liu, H. Zhang, H. Ma, K. Huang, Z. Li, T. Su, A. Vandergriff, J. Tang, T. Allen, P.U. Dinh, J. Cores, Q. Yin, Y. Li, K. Cheng, MicroRNA-21-5p dysregulation in exosomes derived from heart failure patients impairs regenerative potential, J. Clin. Invest. 129 (2019) 2237–2250, doi:10.1172/JCI123135.

[55] T.C.L. Bracco Gartner, J.C. Deddens, E.A. Mol, M. Magin Ferrer, L.W. van Laake, C.V.C. Bouten, A. Khademhosseini, P.A. Doevendans, W.J.L. Suyker, J.P.G. Sluijter, J. Hjortnaes, Anti-fibrotic effects of cardiac progenitor cells in a 3D-model of human cardiac fibrosis, Front. Cardiovasc. Med. 6 (2019) 52, doi:10.3389/fcvm.2019.00052.

[56] N.R. Richbourg, N.A. Peppas, V.I. Sikavitsas, Tuning the biomimetic behavior of scaffolds for regenerative medicine through surface modifications, J. Tissue Eng. Regen. Med. (2019) term.2859, doi:10.1002/term.2859.

[57] J.R. Clegg, A.M. Wagner, S. Ryon Shin, S. Hassan, A. Khademhosseini, N.A. Peppas, Modular fabrication of intelligent material-tissue interfaces for bioinspired and biomimetic devices, Prog. Mater. Sci. (2019) 100589, doi:10.1016/J.PMATSCI.2019.100589.

[58] A Mauretti, S Spaans, N.A.M. Bax, C. Sahlgren, C.V.C. Bouten, Cardiac progenitor cells and the interplay with their microenvironment, Stem Cells Int. (2017) 7471582, doi:10.1155/2017/7471582.